Soft Matter

PAPER

View Article Online
View Journal | View Issue

Open Access Article. Published on 11 November 2025. Downloaded on 1/31/2026 6:07:50 AM.
This article is licensed under a Creative Commons Attribution-NonCommercial 3.0 Unported Licence.

Check for updates

Cite this: *Soft Matter*, 2025, **21**, 9152

Observation of unique stable nano-assemblies of a lipidated glucagon-like peptide 1 analogue

Eva Prada Brichtova,[ab] Ana L. Gomes Dos Santos[c] and Sophie E. Jackson*[a]

Received 5th August 2025,
Accepted 3rd November 2025

DOI: 10.1039/d5sm00801h

rsc.li/soft-matter-journal

Lipidation of glucagon-like peptide 1 (GLP-1) has been widely investigated and utilized as a strategy for the half-life extension of the drug *in vivo*. Several lipidated variants of GLP-1 are used for treatment of type 2 diabetes and obesity and many more are still in development. Lipidated GLP-1 variants show an increased tendency to oligomerize due to their amphiphilic nature. In this work, we report the formation of uniform non-covalent nano-assemblies with vesicular/toroidal morphology which form rapidly by the self-assembly of a lipidated analogue of GLP-1, abbreviated as GLP-1-Am(17, γ-Glu-palm). This analogue shows a high similarity with liraglutide, a commercially available GLP-1-based therapeutic, differing only by the lipidation position shifted by three amino acid residues towards the N-terminus and C-terminal amidation. The formation of vesicular/toroidal assemblies was, nevertheless, reported solely for GLP-1-Am(17, γ-Glu-palm) not for other lipidated analogues studied under the same conditions. The assemblies were formed in a narrow pH range around pH 7.0 and had an average diameter of 21 nm and a high content of α-helical structure. When further incubated at 37 °C with agitation over several days, the assemblies were observed to aggregate into larger amorphous β-structure-rich species. Two distinct kinetic phases of aggregation were observed in the fluorescence assay with ANS dye indicating an accumulation of an aggregation intermediate. We believe that this work demonstrates the morphological diversity of species formed by the self-assembly of an important therapeutic peptide, which may be beneficial especially due to their potential to act as slow-release depots.

Introduction

Glucagon-like peptide 1 (GLP-1) is a peptidic incretin hormone which is secreted by endocrine L cells in the gut in response to food intake and which regulates the glucose level in the blood.[1] The main function of GLP-1 is regulation of insulin exocytosis from pancreatic β-cells. Analogues of GLP-1 are widely used in the treatment of type 2 diabetes.[2] The additional therapeutical benefits of GLP-1-based analogues include weight reduction[3,4] and even lowering of cardiovascular disease risks.[5] The mechanisms of these therapeutic benefits are based on complex changes induced by the peptide on the proteomics level.[6]

Since the native form of GLP-1 has a blood plasma half-life of only approx. 2 min,[7] for therapeutic applications, improvements in the half-life of GLP-1 analogues were needed. Various strategies to prolong the half-life *in vivo* have been investigated including conjugation to human serum albumin, substitution with non-natural amino acids, conjugation to antibodies or attachment of fatty acid moieties.[8–10] The latter strategy of derivatization with fatty acids (lipidation) has proven to be successful for GLP-1 creating two widely commercially-available lipidated analogues: liraglutide and semaglutide, sold under the trademarks Victoza® (also Saxenda®) and Ozempic® (also Rybelsus® or Wegovy®), respectively.[2] Although there has been some progress with oral dosing of GLP-1 analogues, namely semaglutide,[11] the dominant delivery strategy is still injection of an aqueous solution. Therefore, the solution behaviour of these lipidated peptides in storage and *in vivo* is of significant interest.

Lipidated analogues of GLP-1 have been observed to self-assemble into oligomeric species the nature of which differs depending on the position of the lipidation site and the type of linker and lipid moiety used.[12] Liraglutide, for instance, is known to form distinct oligomeric species,[13,14] the populations of which can be regulated by pH.[15] The observed self-assembly into oligomers contributes to the improved half-life of GLP-1 analogues as increasing the size of the species together with its binding to human serum albumin both prevent rapid renal clearance.[8] However, lipidated (as well as non-lipidated) GLP-1 analogues have also been observed to be prone to aggregate

[a] *Yusuf Hamied Department of Chemistry, University of Cambridge, Cambridge, CB2 1EW, UK. E-mail: sej13@cam.ac.uk*
[b] *Institute of Chemical, Environmental and Bioscience Engineering, Technische Universität Wien, Gumpendorferstraße 1A, Vienna, 1060, Austria*
[c] *Advanced Drug Delivery, Pharmaceutical Sciences, R&D, AstraZeneca, Biomedical Campus, Cambridge, CB2 0AA, UK*

 This journal is © The Royal Society of Chemistry 2025

Open Access Article. Published on 11 November 2025. Downloaded on 1/31/2026 6:07:50 AM.
This article is licensed under a Creative Commons Attribution-NonCommercial 3.0 Unported Licence.

into amyloid-like fibrillar or amorphous aggregates.[12] This process is usually accompanied by a change in the secondary structure of the peptide and a loss of a biological activity, although reversible formation of nanofibers has been reported as well.[16] In addition, semaglutide was shown to be prone to another solution-based instability – surface-catalyzed emulsification; *i.e.*, formation of stable colloidal droplets which is not accompanied by a change in the peptide's secondary structure.[17] Other study reports a formation of stable oligomeric micelles of semaglutide.[18] A further example of morphological diversity of aggregates and reversibly self-assembled species of lipidated peptides and proteins includes glutamic acid-rich lipopeptide, which is capable of self-assembly into nanofibers or micelles in blood serum in the pH range between 7.0 and 7.4.[19] Another example is a peptide conjugate consisting of a heptapeptide sequence for which the formation of either spherical micelles or nanofibers is regulated by temperature.[20]

Self-assembly of amphiphilic molecules into toroidal species has been reported both in natural and artificially designed systems.[21] Toroidal nanostructures can be defined as symmetrical ring-shaped structures with a central pore. Many transmembrane proteins such as β-barrels and α-helical bundles have toroidal shapes.[21] Toroidal motifs have also been observed in so called "amyloid pores" formed by amyloid-β peptide which is associated with neurodegenerative diseases.[22] The formation of highly uniform, β-sheet-rich and discrete toroidal nanostructures was reported for an artificially designed short peptide consisting of alternating hydrophobic and hydrophilic segments.[23] Interestingly, in this case, higher pH led to the formation of nanoribbons which were reversibly transformed into toroidal nanostructures after acidifying the solution to pH ≅ 7.[23] Coexistence of toroidal structures and β-ribbon structures was also reported in the self-assembly of rationally designed block copolypeptides consisting of non-β-sheet poly(L-arginine) and β-sheet segments.[24] In this case, an increase in salt concentration, resulted in the toroidal structures dominating over other species. The resulting toroidal structures had a highly uniform diameter of about 10 nm, indicating the existence of a preferred geometrical packing for the formation of the toroidal morphology.[24] Another example is a peptide macrocycle which was designed to contain a hydrophobic β-sheet-forming segment and an α-helical region connected *via* linkers. The stabilization of the α-helical structure was achieved only upon self-assembly of the peptide macrocycles into toroidal nanostructures where the hydrophobic β-sheet-forming segments were in the central pore whereas the α-helical segments formed the outer part of the toroid.[25]

Our previous research showed that the lipidation of GLP-1 greatly influences the solubility, oligomerization and aggregation behaviour of the peptide.[12] All these properties are regulated by both the position of the lipidation site in the peptide sequence as well as the nature of the lipid moiety and the linker used to attach the lipid to the peptide. In this work, we report an unusual self-assembly into regular vesicular/toroidal species of a GLP-1 analogue which is lipidated using palmitic acid connected *via* γ-glutamic acid linker at Lys17 side chain – GLP-1-Am(17, γ-Glu-palm), the structure of which is depicted in Fig. 1(A) and (B). This GLP-1 analogue shows a high degree of similarity with liraglutide, GLP-1-based therapeutic, sold under commercial trademarks Victoza® and Saxenda®. GLP-1-Am(17, γ-Glu-palm)

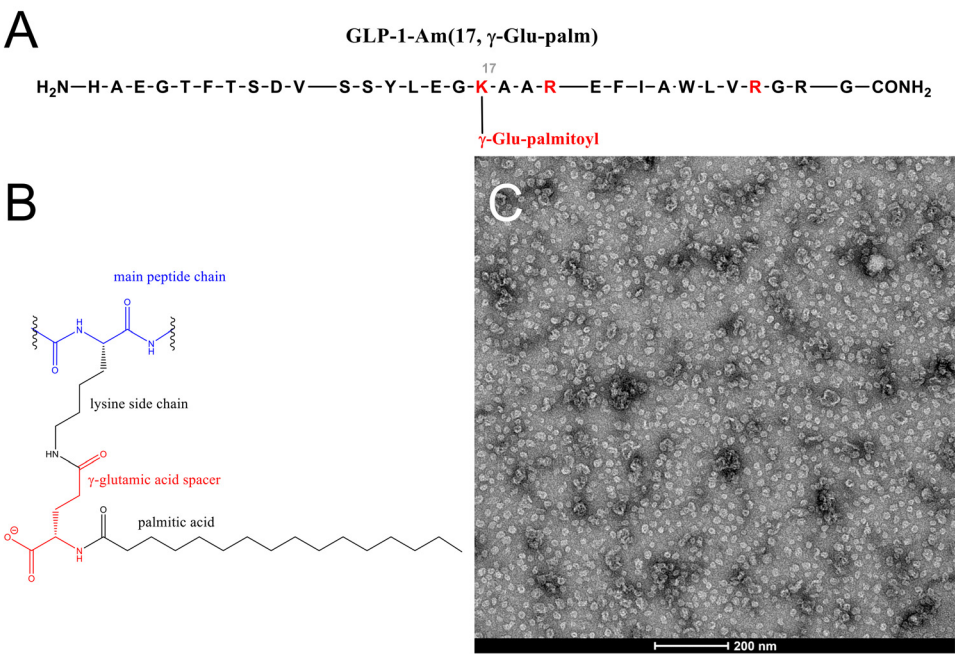

Fig. 1 GLP-1-Am(17, γ-Glu-palm) structure and self-assembled species formed at pH 7.0. Sequence of GLP-1-Am(17, γ-Glu-palm) – panel A. The position of the lipidation site is numbered and highlighted in red. Additionally, the substitution sites relative to GLP-1-Am are highlighted in red. Detailed structure of the lipidation and attachment site (B). Population of assemblies formed by freshly prepared 40 μM GLP-1-Am(17, γ-Glu-palm) in 25 mM phosphate at pH 7.0 imaged by transmission electron microscopy (C).

Open Access Article. Published on 11 November 2025. Downloaded on 1/31/2026 6:07:50 AM.
This article is licensed under a Creative Commons Attribution-NonCommercial 3.0 Unported Licence.

contains the same lipidation and linker moiety and differs only by the lipidation position shifted by three amino acid residues towards the N-terminus, as well as C-terminal amidation. Here, we show that a highly uniform population of a vesicular/toroidal species of GLP-1-Am(17, γ-Glu-palm) formed rapidly and solely in a narrow pH range around pH 7.0. The assemblies formed were characterized in terms of their uniformity, size, structure and stability in solution. The behaviour of GLP-1-Am(17, γ-Glu-palm) was compared to other GLP-1 lipidated analogues, GLP-1-Am(12, γ-Glu-palm) and GLP-1-Am(20, γ-Glu-palm), however, the existence of these uniform nano-assemblies was reported solely for GLP-1-Am(17, γ-Glu-palm).

Results and discussion

Lipidated GLP-1 analogue forms a uniform population of assemblies at pH 7.0

As was reported in our previous study,[12] GLP-1-Am(17, γ-Glu-palm) is soluble only at pH values above 7.0 with a limited solubility (reaching maximum peptide concentration of 50 μM) at pH close to 7.0. A sample of freshly prepared 40 μM GLP-1-Am(17, γ-Glu-palm) in 25 mM phosphate at pH 7.0 was imaged using transmission electron microscopy with uranyl acetate staining (Fig. 1(C)). Under these conditions, a uniform population of regular spherical species was observed. This behaviour occurs only close to pH 7.0 as already at pH 7.5, GLP-1-Am(17, γ-Glu-palm) was shown to form diverse populations of smaller oligomers.[12]

The observed pH-induced transition from regular spherical assemblies at pH 7.0 to oligomeric species at pH 7.5, is likely to be associated with deprotonation of either the N-terminus or His1 side chain as those groups have pK_a values in the right pH range.[26] Therefore, it is likely that the N-terminal histidine residue plays a crucial role both in the solubility and self-assembly properties of GLP-1 analogues.

Observed assemblies have a vesicular or toroidal morphology and a high content of α-helical structure

As observed by negatively-stained TEM with higher magnification (Fig. 2(A)), GLP-1-Am(17, γ-Glu-palm), indeed, forms assemblies with a spherical shape with a hollow cavity in the middle resembling a toroid. A sample prepared under the same conditions (40 μM peptide concentration in 25 mM phosphate at pH 7.0) was also imaged using cryo-EM to eliminate the effect of staining and drying on the grid during sample preparation which can be potentially damaging for the sample. Fig. 2(B) shows that the morphology of assemblies imaged using cryo-EM is similar to assemblies which were imaged using negative staining TEM. Therefore, the staining and drying process is not likely to cause significant disruption of the morphology of the observed GLP-1-Am(17, γ-Glu-palm) assemblies. The hydrophobic core of GLP-1-Am(17, γ-Glu-palm) assemblies is likely to be formed by the palmitic acid aliphatic chains whereas the charged hydrophilic parts of the peptide chain are likely to be on the outer surface of the assembly. Lipidated peptides are known to form well-defined spherical micelles, however, the diameter of observed assemblies of GLP-1-Am(17, γ-Glu-palm) is too large to correspond to a single-layer micelle, for which the diameter would be expected to be lower than 5 or 6 nm.[27] The diameter of the assemblies shown in Fig. 2 is in the size range of 12–27 nm with a hollow cavity in the middle of about half the size of the assembly. These dimensions could correspond to a bilayer vesicular structure with the hydrophobic area in between two hydrophilic layers excluded from solvent. Solely from TEM images it is not distinguishable whether the assemblies formed are of a toroidal morphology or are vesicles (*i.e.*, bilayer-based nanostructures).

The size-uniformity of GLP-1-Am(17, γ-Glu-palm) species formed at pH 7.0 was also analyzed by size-exclusion chromatography. Chromatograms measured at multiple peptide concentrations, Fig. 3(A), show only a single peak eluting at around 8 mL. This observation indicates the formation of a single

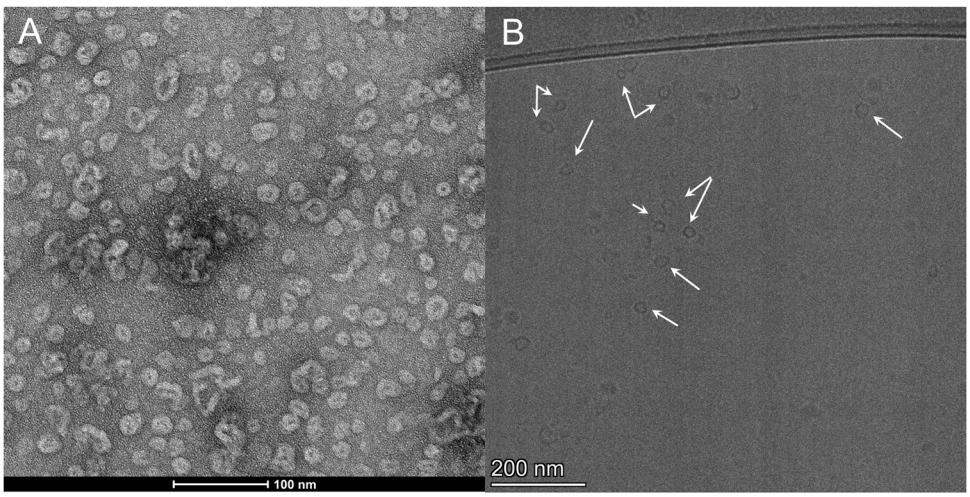

Fig. 2 Assemblies of GLP-1-Am(17, γ-Glu-palm) imaged by electron microscopy. TEM (A) and cryo-EM (B) images of assemblies formed at pH 7.0. The samples for electron miscroscopy were freshly prepared at 40 μM peptide concentration in 25 mM phosphate, pH 7.0, at room temperature.

Open Access Article. Published on 11 November 2025. Downloaded on 1/31/2026 6:07:50 AM.
This article is licensed under a Creative Commons Attribution-NonCommercial 3.0 Unported Licence.

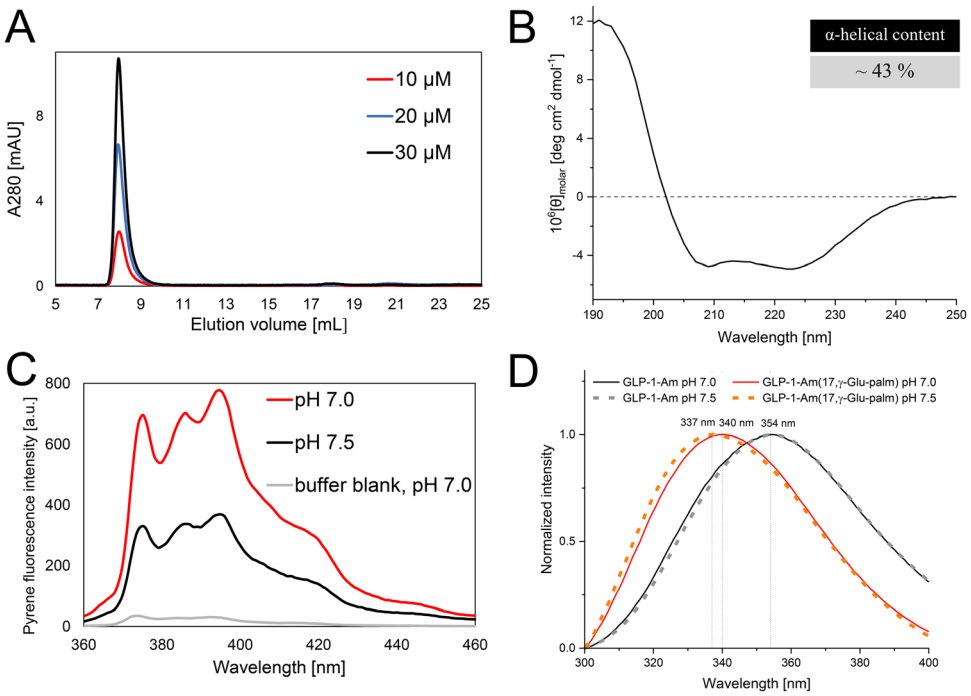

Fig. 3 Biophysical characterization of GLP-1-Am(17, γ-Glu-palm) assemblies formed at pH 7.0. Size-exclusion chromatograms of GLP-1-Am(17, γ-Glu-palm) samples at 10, 20 and 30 μM concentration freshly prepared in 25 mM phosphate, pH 7.0 (A). 40 μM GLP-1-Am(17, γ-Glu-palm) freshly prepared in 25 mM phosphate at pH 7.0 was characterized using far-UV CD. Total α-helical content predicted by far-UV CD was calculated as indicated in Materials and Methods (B). The presence of vesicular/toroidal assemblies was assessed using the pyrene assay as the pyrene fluorescence intensity increases in a more hydrophobic environment. 50 μM GLP-1-Am(17, γ-Glu-palm) samples freshly prepared in 25 mM phosphate at pH 7.0 and 7.5 with 1 μM pyrene were tested with the fluorescence intensity being two times higher at pH 7.0 where vesicular/toroidal assemblies were observed (C). Intrinsic tryptophan fluorescence spectra were recorded after an excitation at 280 nm for freshly prepared 50 μM GLP-1-Am(17, γ-Glu-palm) samples at pH 7.0 and 7.5 and 50 μM non-lipidated GLP-1-Am under the same conditions (D). All experiments shown in A–D were performed at room temperature.

species which is stable and independent of peptide concentration under the conditions used. Using a calibration curve for the size-exclusion column (Table S1 and Fig. S1B), the diameter of eluted species was estimated to be *circa* 21 nm which fits well with the size range observed by TEM and cryo-EM. This size corresponds to approximately 210 monomeric units of GLP-1-Am(17, γ-Glu-palm) as estimated from size-exclusion chromatography calibration curve (Fig. S1A). At pH values higher than 7.0, the size distribution of observed species vastly differs – the oligomeric species formed at pH 7.5, 8.0 and 8.5 show much lower hydrodynamic radius (*i.e.*, smaller size) and their distribution is no longer uniform with the species of various sizes being populated as depicted in Fig. S2.

The peptide conformation within assemblies observed at pH 7.0 was characterized using far-UV circular dichroism (CD). The far-UV CD spectrum of freshly prepared solution of GLP-1-Am(17, γ-Glu-palm) at pH 7.0 has two minima at around 222 nm and 210 nm (Fig. 3(B)). The secondary structure prediction shows a high content of α-helix of about 43% in the assembly. The high content of α-helix has been already reported in a micelle-like structure of a PEGylated and lipidated gut-derived peptide hormone[28,29] and nanotubular assembly of lysine-rich lipopeptide.[30] Moreover, the increase in α-helicity of the peptidic part upon lipidation has been reported for multiple therapeutic peptides.[12,31] Due to the instant formation of these assemblies and their high content of α-helical structure, it is unlikely that they are formed by cyclization of amyloid fibrils (so called "amyloid loops"), which have been observed for other proteins in previous studies.[32–34] The presence of α-helical regions in the structure of GLP-1 and GLP-1-based analogues was previously reported in solution *in vitro*[35,36] as well as *in vivo* with the cryo-EM structure of GLP-1 bound to its receptor.[37] Moreover, some degree of α-helicity is likely to be present already in the lyophilized state of synthetically prepared GLP-1 analogues including GLP-1-Am(17, γ-Glu-palm) as shown by FTIR spectra, Fig. S3. Therefore, it can be assumed that the structure of GLP-1-Am(17, γ-Glu-palm) within these assemblies is rather "native-like".

The self-assembly behaviour of GLP-1-Am(17, γ-Glu-palm) was further investigated using a pyrene assay. Pyrene fluorescence is sensitive to the solvent environment as its intensity increases when pyrene is in a more hydrophobic environment, *e.g.*, into the hydrophobic core of a micelle or oligomer. This assay is, therefore, often employed to detect the critical micelle/aggregation concentration and/or the presence of micelle-like oligomers in systems. Fluorescence emission spectra of 50 μM GLP-1-Am(17, γ-Glu-palm) with 1 μM pyrene at pH 7.0 and 7.5 were recorded (Fig. 3(C)). GLP-1-Am(17, γ-Glu-palm) shows a significantly higher pyrene fluorescence intensity at pH 7.0 compared to pH 7.5. These findings were reproducible and

Open Access Article. Published on 11 November 2025. Downloaded on 1/31/2026 6:07:50 AM.
This article is licensed under a Creative Commons Attribution-NonCommercial 3.0 Unported Licence.

independent of the ionic strength or buffer used (Fig. S4). Moreover, higher pyrene fluorescence intensity values were recorded solely at pH 7 not at other pH values tested (pH 7.5, 8.0 and 8.5; Fig. S4). This observation corresponds with the formation of spherical assemblies exclusively at pH 7.0 and indicates that the presence of assemblies increases pyrene fluorescence to a greater degree than smaller oligomers of GLP-1-Am(17, γ-Glu-palm) formed at different pH conditions. This is likely due to the penetration of pyrene into the highly hydrophobic interior of the vesicle/toroid. The pyrene assay was also performed over a range of peptide concentrations from 2 to 50 μM at pH 7.0, however, the analysis of the fluorescence emission intensity at 373 nm did not show any critical concentration for the formation of the observed assemblies in this concentration range (Fig. S5). Therefore, these results suggest that the critical micellar concentration for GLP-1-Am(17, γ-Glu-palm) at pH 7.0 is below 2 μM and, therefore, that the observed assemblies are stable at all the concentrations tested in this study. Additionally, the presence of vesicular/toroidal assemblies at pH 7.0 and smaller non-vesicular/toroidal oligomers at pH 7.5 can be observed in the difference in absorption spectra of freshly prepared samples at the same GLP-1-Am(17, γ-Glu-palm) concentration under both conditions. At pH 7.0, a significantly higher level of light scattering in the sample was observed compared to the sample at pH 7.5 (Fig. S6) which is due to the presence of larger particles, *i.e.*, vesicular/toroidal assemblies.

Intrinsic tryptophan fluorescence spectrum (Fig. 3(D)) of a freshly prepared solution of GLP-1-Am(17, γ-Glu-palm) at pH 7.0 shows a maximum (λ_{max}) at 340 nm implying that the tryptophan residue (Trp25) is more buried in the assembled structure compared to the non-lipidated GLP-1-Am studied under the same conditions (λ_{max} = 354 nm). The tryptophan fluorescence spectrum for assemblies populated at pH 7.0 is, nevertheless, comparable to the spectrum measured for smaller oligomers of GLP-1-Am(17, γ-Glu-palm) populated at pH 7.5 where λ_{max} reaches 337 nm as depicted in Fig. 3(D).

The formation of vesicular/toroidal assemblies appears to be highly sensitive to the charge state of GLP-1-Am(17, γ-Glu-palm) as the assemblies were observed only close to pH 7.0. GLP-1-Am(17, γ-Glu-palm) was observed to be soluble only at the pH range where its net charge is negative, *i.e.* pH ≥ 7.0. The formation of these assemblies has, therefore, been reported in "the transition pH-range" where the analogue starts to be soluble. Close to pH 7.0, the net charge of the analogue is around −1, going higher in pH, there is an increase in the negative net charge as the N-terminus starts to get deprotonated. This deprotonation and the increase in negative net charge are likely to be responsible for the disruption of vesicular/toroidal morphology. The plot illustrating the theoretical net charge values development with pH is given in Fig. S7. In addition, the formation of assemblies is highly dependent on the position where the linker with lipid is attached since the structurally similar GLP-1-Am(12, γ-Glu-palm) and GLP-1-Am(20, γ-Glu-palm) with similar solubility ranges but differing in the position of the lipidation did not show the same behaviour but formed smaller non-vesicular/toroidal oligomers under the same conditions – Fig. S8.

The largely α-helical structure, resembling the conformation of GLP-1 upon binding to its receptor, of the peptide analogue in the observed assembly together with the stability of the assembly in solution may provide an interesting concept for a slow-release long-acting drug formulation. It is unlikely that the large assemblies themself can directly bind to the receptor. They are very likely to coexist in a dynamic equilibrium where the large oligomeric species are dominant, but they are capable of dissociation into smaller oligomers and monomers which are present at lower concentrations – these then interact with the receptor. Evidence for such an equilibrium/equilibria is observable in the magnified size-exclusion chromatograms where trace concentrations of small oligomers and monomers can be seen, Fig. S9.

Physical stability of assemblies formed at pH 7.0

The stability of observed assemblies was investigated using TEM imaging of samples incubated in 25 mM phosphate buffer, pH 7.0, at 37 °C with continuous agitation for eight days. TEM imaging reveals that the smaller regular vesicular/toroidal assemblies slowly convert to larger irregular vesicular/toroidal species, in addition to forming large amorphous aggregates (Fig. 4(A)). These large aggregates can be hypothetically formed by short curly fibres, however, they show clear structural differences in comparison to aggregates formed during aggregation at higher pH values where the population of smaller oligomers gradually aggregates into thread-like structures, most likely amyloid fibrils (Fig. S10). As determined from TEM images of GLP-1-Am(17, γ-Glu-palm) at pH 7.0, the diameter of larger irregular species is between 70 and 90 nm whereas the diameter of initial assemblies is in the range of 12–27 nm. Since the initial vesicular/toroidal assemblies elute as a single symmetrical peak on SEC (Fig. 3(A)) with the size corresponding to *circa* 21 nm, it is likely that their size is rather uniform and the broader size range obtained from TEM images is given by the technical limitations of the method and sample preparation (drying the sample on a grid and staining).

The aggregation of GLP-1-Am(17, γ-Glu-palm) assemblies formed at pH 7.0 was also monitored using size-exclusion chromatography. Fig. 4(B) shows the chromatograms of GLP-1-Am(17, γ-Glu-palm) in 25 mM Tris, pH 7.0, at different time points after incubation at 37 °C with continuous shaking. The UV trace of a freshly prepared sample (in black) shows a single intense peak eluting at around 9.5 mL corresponding to a homogeneous population of initial vesicular/toroidal assemblies. Over time, a second peak eluting in the void volume of the column appears which indicates the formation of larger species, presumably the larger hollow species and/or amorphous aggregates observed by TEM, Fig. 4(A). After 72 hours of incubation at 37 °C, the ratio of species eluting at 9.5 mL and in the void volume was approximately equal indicating the existence of multiple species in the sample.

The ageing of 50 μM GLP-1-Am(17, γ-Glu-palm) in 25 mM phosphate buffer at pH 7.0 was monitored using 8-anilino-naphthalene-1-sulfonic acid (ANS) and thioflavin T (ThT)

Open Access Article. Published on 11 November 2025. Downloaded on 1/31/2026 6:07:50 AM.
This article is licensed under a Creative Commons Attribution-NonCommercial 3.0 Unported Licence.

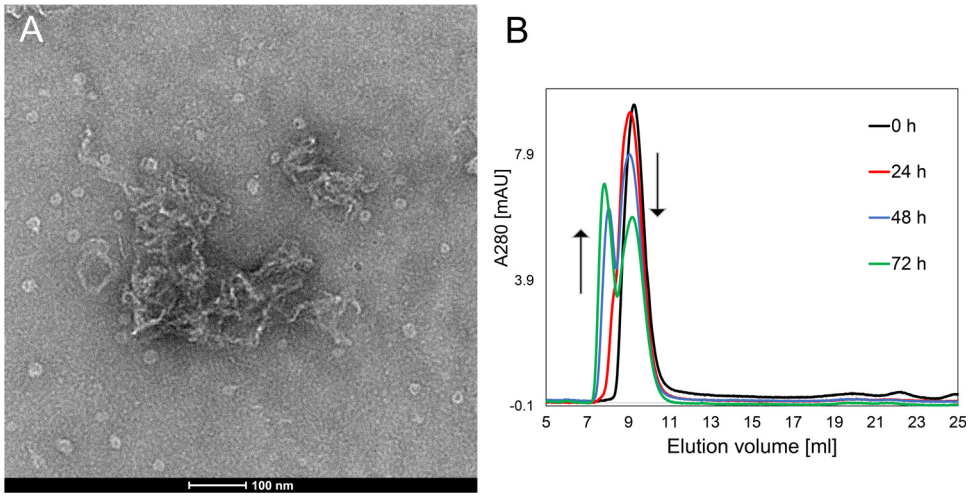

Fig. 4 Aggregation of vesicular/toroidal assemblies into larger amorphous species. A sample of 40 μM GLP-1-Am(17, γ-Glu-palm) in 25 mM phosphate buffer at pH 7.0 incubated for 8 days at 37 °C with continuous agitation was applied onto a carbon-coated copper grid, stained with 2% uranyl acetate and imaged using transmission electron microscopy (A). Samples of 40 μM GLP-1-Am(17, γ-Glu-palm) in 25 mM Tris at pH 7.0 were injected at different time points, of their incubation at 37 °C with continuous agitation, onto a size-exclusion column Superdex 200 Increase 10/300 (B). The size-exclusion chromatography was performed at room temperature.

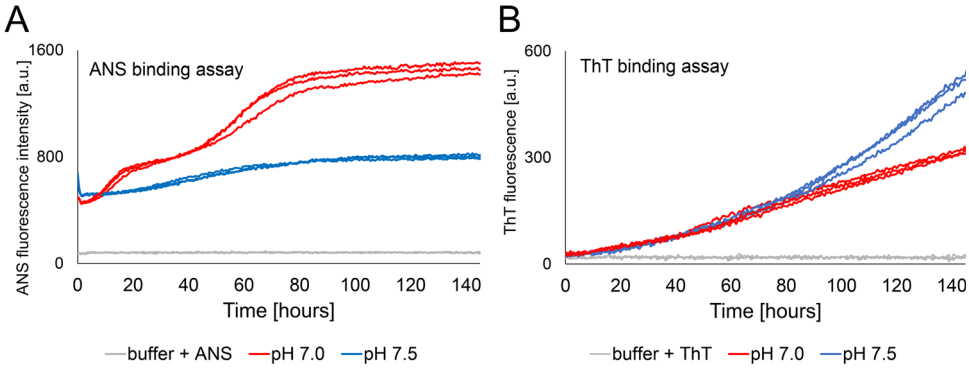

Fig. 5 Ageing and physical stability of GLP-1-Am(17, γ-Glu-palm) at pH 7.0 monitored by ANS and ThT fluorescence assays. Assays were performed in 25 mM phosphate at pH 7.0 and 7.5 with either 250 μM ANS (A) or 50 μM ThT (B). Samples of 50 μM GLP-1-Am(17, γ-Glu-palm) were incubated for 145 hours at 37 °C with periodic agitation and readings were taken every 30 minutes. Each sample was measured in triplicate within the same plate.

assays. Under these conditions, the freshly prepared sample consists of initial vesicular/toroidal assemblies of a uniform size. Fig. 5(A) shows the results of an ANS fluorescence assay with 50 μM GLP-1-Am(17, γ-Glu-palm) at pH 7.0 and pH 7.5 over six days at 37 °C with periodic agitation. The ANS curve obtained at pH 7.0 differs from the one obtained at pH 7.5 in both its fluorescence intensity and shape. Two distinct kinetic phases are apparent at pH 7.0, which may correspond to (i) the conversion of the initial assemblies (*circa* 21 nm) into larger hollow species (70–90 nm) and (ii) the subsequent aggregation of these species into amorphous aggregates as depicted in Fig. 4(A). Each kinetic phase is preceded by a lag phase suggesting the occurrence of lower-ANS-binding intermediates which then convert to higher-ANS-binding states. Fig. 5(B) shows the aggregation kinetics of 50 μM GLP-1-Am(17, γ-Glu-palm) at pH 7.0 and 7.5 as probed by ThT fluorescence over six days at 37 °C with periodic shaking. Unlike in the ANS assay (Fig. 5(A)), only a single phase is observed in the ThT assay corresponding to a slow increase of ThT fluorescence emission over time, suggesting an increase in β-structure over time. A steady increase in ThT fluorescence over time was also observed for the sample prepared at pH 7.5 suggesting the formation of β-structure also during ageing of smaller oligomers. Together with the formation of larger species of GLP-1-Am(17, γ-Glu-palm) observed in TEM images and SEC (Fig. 4), the results obtained from the ThT assay (Fig. 5(B)) and circular dichroism (Fig. S11) show gradual aggregation of initial assemblies which is accompanied by an increase in β-structure during the sample ageing.

Materials and methods

Peptide samples

GLP-1-Am, H-HAEGTFTSDVSSYLEGQAAKEFIAWLVKGRG-NH_2, molecular weight (M_W) of 3355 Da, was purchased from

Open Access Article. Published on 11 November 2025. Downloaded on 1/31/2026 6:07:50 AM.
This article is licensed under a Creative Commons Attribution-NonCommercial 3.0 Unported Licence.

GenScript in the form of an acetate salt with 99.2% purity and stored as a lyophilized powder.

GLP-1-Am(12, γ-Glu-palm), H-HAEGTFTSDVSK(γ-Glu-palmitoyl)YLEGQAAREFIAWLVRGRG-NH_2, M_W: 3819 Da, was purchased from Bachem in the form of an acetate salt with 95.6% purity and stored as a lyophilized powder.

GLP-1-Am(17, γ-Glu-palm), H-HAEGTFTSDVSSYLEGK(γ-Glu-palmitoyl)AAREFIAWLVRGRG-NH_2, M_W: 3778 Da, was purchased from Bachem in the form of an acetate salt with 96.3% purity and stored as a lyophilized powder.

GLP-1-Am(20, γ-Glu-palm), a C-terminally amidated liraglutide analogue: H-HAEGTFTSDVSSYLEGQAAK(γ-Glu-palmitoyl)EFIAWLVRGRG-NH_2; M_W: 3750 Da, was purchased from Peptides International in the form of an acetate salt with > 96% purity and stored as a lyophilized powder.

Sample preparation and sample ageing

Fresh samples were prepared by dissolving the lyophilized peptide powder in a corresponding buffer and subsequent filtration of the sample through a 0.22 μm syringe filter (PES membranes, Millex). The concentration of the peptide in the filtered solution was determined spectrophotometrically using the Beer–Lambert Law and a theoretical extinction coefficient of 6990 M^{-1} cm^{-1} at 280 nm (ε_{280}). When light scattering of the sample was observed as a significant absorbance at 320 nm (A_{320}), the concentration was calculated using the scattering-corrected expression:

$$c = \frac{A_{280} - 1.929A_{330}}{\varepsilon_{280} \cdot l}$$

where c is the concentration in mol L^{-1} and l is the pathlength of the cuvette in cm, here $l = 1$.

Samples for long-term ageing experiments were either incubated in a 96-well half-area plate (Corning 3881) or in 1.5 mL plastic microcentrifuge tubes (STARLAB) sealed or wrapped in aluminium foil to protect from sunlight. The incubation was performed at 37 °C with periodic 180 rpm agitation in a FLUOstar Omega microplate reader (BMG Labtech) or in an Incubator Shaker (Innova® 43) at 37 °C with continuous 180 rpm agitation.

Transmission electron microscopy (TEM) and cryo-EM

Samples were imaged using a Thermo Scientific Talos F200X G2 Transmission Electron Microscope with an acceleration voltage of 200 kV. 2 μL of the sample was loaded onto carbon-coated 300 mesh copper grid (EMResolutions or Agar Scientific), which was glow discharged using a Quorum Technologies GloQube system prior to sample application. The sample was dried by blotting, then negatively stained with 2 μL of 2% (w/w) uranyl acetate solution for 15–30 seconds and dried again.

Samples for cryo-EM were filtered through a 0.22 μm membrane filter, applied onto a lacey carbon-coated TEM 300 mesh copper grid and plunge-frozen in liquid ethane. Before sample application, the grids were glow discharged using a Quorum Technologies GloQube system. 3 μL of the samples were pipetted onto a TEM grid, blotted for 3 s at blot force −5 using dedicated filter paper, and immediately plunged into liquid ethane using a Vitrobot Mark IV with a chamber set to 4 °C and 95% humidity. Samples after vitrification were kept under liquid nitrogen until they were inserted into a Gatan Elsa cryo holder and imaged at −178 °C. Images were collected using a Thermo Scientific (FEI) Talos F200X G2 microscope at 200 kV at low dose using a Ceta 16M CMOS camera and Velox software.

Size-exclusion chromatography

Analytical size-exclusion chromatography was performed on an ÄKTA FPLC system (GE Healthcare), using a Superdex 200 Increase 10/300 column (GE Healthcare). Samples were loaded using a 200 μL loop. Prior to loading, the samples were filtered through a 0.22 μm filter (Millex, PVDF Membrane) to avoid blocking of the column by large aggregates. All samples were eluted at a flow rate of 0.75 mL min^{-1} at room temperature and UV absorbance detection at 280 nm through a 0.5 cm flow cell was used. A set of globular protein standards (GE Healthcare) was used to construct a calibration curve for the column – Table S1 and Fig. S1.

Circular dichroism

Circular dichroism (CD) spectra were measured on a Chirascan CD spectrometer (Applied Photophysics). Far-UV CD spectra were measured in a 1 mm pathlength cuvette and the measurement was performed with a 1 nm step size and with a 1 nm spectral bandwidth. The resulting spectrum was obtained as an average of three scans and the spectrum of the pure buffer was subtracted. All measurements were performed at room temperature. The CD machine units (ellipticity – signal expressed in mdeg) were converted to molar ellipticity $[\theta]_{molar}$ using the following equation:

$$[\theta]_{molar} = \frac{m^0}{10 \cdot l \cdot c}$$

where $[\theta]_{molar}$ is the molar ellipticity (with units deg cm^2 $dmol^{-1}$), m^0 is the CD signal in mdeg (machine units), l is the cuvette pathlength in cm, and c is the sample concentration in mol L^{-1}.

α-helical content was estimated using mean residue ellipticity value at 222 nm (MRE_{222}), which was calculated as follows:

$$MRE_{222} = \frac{m^0_{222}}{10 \cdot l \cdot c \cdot n}$$

where m^0_{222} is the CD signal in mdeg (machine units) at 222 nm, l is the cuvette pathlength in cm, c is the sample concentration in mol L^{-1}, and n is the number of amino acid residues. α-Helical content was estimated using a method based on a liner interpolation between experimentally determined MRE_{222} values for purely α-helical and purely coiled protein.[42–44] α-Helical content is then calculated as:

$$\%\ \text{helicity} = 100 \times \left(1 + \frac{(MRE_{222} - MRE_{helix})}{(MRE_{coil} - MRE_{222})}\right)^{-1}.$$

where MRE_{222} is the observed ellipticity at 222 nm, MRE_{helix} is the value for purely α-helical structure (−35 791 deg cm^2 $dmol^{-1}$,

 This journal is © The Royal Society of Chemistry 2025

Open Access Article. Published on 11 November 2025. Downloaded on 1/31/2026 6:07:50 AM.
This article is licensed under a Creative Commons Attribution-NonCommercial 3.0 Unported Licence.

at 25 °C), and MRE_{coil} is the value for purely coiled structure (−725 deg cm^2 $dmol^{-1}$, at 25 °C).[44]

Pyrene assay

The presence of toroidal assemblies in GLP-1-Am(17, γ-Glu-palm) samples was probed based on changes in pyrene fluorescence. Pyrene from a stock solution (197.6 μM pyrene concentration in 70% methanol solution) was added to the peptide sample such that the final concentration of pyrene in the sample was 1 μM. Fluorescence spectra were recorded using a Cary Eclipse fluorescence spectrophotometer (Agilent Technologies). Samples were measured in a 120 μL quartz cuvette (Hellma Analytics). The excitation wavelength was 339 nm and the emission spectra were collected between 360 nm and 460 nm in 1 nm steps. The emission and excitation band passes were 5 nm and the voltage on the photomultiplier tube was 600 V. Measurements were carried out at room temperature.

Intrinsic tryptophan fluorescence

Intrinsic tryptophan fluorescence spectra were measured on a Cary Eclipse fluorescence spectrophotometer (Agilent Technologies). Spectra were obtained using an excitation wavelength of 280 nm and emission spectra were recorded between 300 and 400 nm with a step of 1 nm. Emission and excitation band passes of 10 nm, and a voltage on the photomultiplier tube of 550 V were used. Samples were measured in a 120 μL quartz cuvette (Hellma Analytics). Measurements were carried out at room temperature.

8-Anilinonaphthalene-1-sulfonic acid (ANS) fluorescence assay

The ageing of toroidal assemblies was probed using 8-anilino-1-naphthalenesulfonic acid (ANS) fluorescent dye which binds to exposed hydrophobic patches. Samples were prepared in the wells of a 96-well half-area plate (Corning 3881) by mixing the peptide samples with ANS to a total volume of 120 μL, in which the final concentration of the ANS dye was 250 μM and the concentration of GLP-1-Am(17, γ-Glu-palm) was 50 μM. To prevent evaporation of the samples, the plate was sealed with tape (Costar Thermowell). The fluorescence measurements were performed using a FLUOstar Omega (BMG Labtech) plate reader, with an excitation filter at 355 nm and an emission filter at 482 nm, at a gain of 500 and 8 flashes per well. The plate was incubated at 37 °C and readings were taken through the bottom of the wells every 35 minutes, after 5 minutes of shaking at 600 rpm, over six days. Each sample was measured in triplicate.

Thioflavin T (ThT) fluorescence assay

The stability of vesicular/toroidal assemblies over six days at 37 °C was monitored *via* ThT fluorescence assays using a FLUOstar Omega microplate reader (BMG Labtech). Samples of 50 μM GLP-1-Am(17, γ-Glu-palm) with ThT of the total concentration of 50 μM were pipetted into a 96-well half-area plate (Corning 3881) and sealed with tape (Costar Thermowell) to prevent samples from evaporating. The total volume of sample in each well was 120 μL. Bottom reading of the plate was performed every 30 minutes with five minutes of shaking prior to each reading (orbital shaker mode at 600 rpm). ThT fluorescence emission at 482 nm was recorded after excitation at 448 nm. Fluorescence was measured at a gain of 500 with 8 flashes per well.

Conclusions

In this work, we reported the formation of non-covalent vesicular/toroidal assemblies of a lipidated GLP-1 analogue, GLP-1-Am(17, γ-Glu-palm) structurally very similar to commercially-available therapeutic liraglutide. The observed assemblies are formed in a narrow pH range, close to pH 7.0. Under these conditions, the solubility of GLP-1-Am(17, γ-Glu-palm) is limited and a uniform population of hollow spherical assemblies with an average diameter of about 20 nm was formed in solution. This phenomenon occurs only in a narrow pH range at around pH 7.0 and was reported only for GLP-1-Am(17, γ-Glu-palm) analogue as the other analogues tested, GLP-1-Am(12, γ-Glu-palm) and GLP-1-Am(20, γ-Glu-palm), did not show this behaviour. The reported assemblies of GLP-1-Am(17, γ-Glu-palm) have a high content of α-helical structure and they are stable over several hours at room temperature and also at 37 °C. When incubated at 37 °C with periodic agitation, these assemblies further aggregate into larger vesicular/toroidal species and later into amorphous aggregates. This process is accompanied with an increase in β-structure. These observations, together with other studies,[21,28,38–41] show that various micellar structures, vesicles and toroidal assemblies of amphiphiles are another class of stable species which may occur as a result of self-assembly. Moreover, it highlights the dependency of the morphology of self-assembly/oligomers of lipidated GLP-1 analogues on both pH and the site of lipidation.

Conflicts of interest

The authors declare the following competing financial interest(s): Ana L. Gomes Dos Santos is an employee of AstraZeneca, Cambridge.

Data availability

The data supporting this article have been included as part of the supplementary information (SI). Supplementary information is available. See DOI: **https://doi.org/10.1039/d5sm00801h**.

Acknowledgements

E. P. B. was supported by a PhD studentship from Peterhouse, Cambridge. Authors would like to thank Dr Heather Greer for her assistance with TEM and cryo-TEM and financial support by EPSRC Underpinning Multi-User Equipment Call (EP/P030467/1).

Open Access Article. Published on 11 November 2025. Downloaded on 1/31/2026 6:07:50 AM.
This article is licensed under a Creative Commons Attribution-NonCommercial 3.0 Unported Licence.

References

1 J. J. Holst, The Physiology of Glucagon-like Peptide 1, *Physiol. Rev.*, 2007, **87**, 1409–1439, DOI: 10.1152/physrev.00034.2006.

2 M. Yu, M. M. Benjamin, S. Srinivasan, E. E. Morin, E. I. Shishatskaya, S. P. Schwendeman and A. Schwendeman, Battle of GLP-1 Delivery Technologies, *Adv. Drug Delivery Rev.*, 2018, **130**, 113–130, DOI: 10.1016/j.addr.2018.07.009.

3 S. S. Torekov, S. Madsbad and J. J. Holst, Obesity – an Indication for GLP-1 Treatment? Obesity Pathophysiology and GLP-1 Treatment Potential: Obesity – an Indication for GLP-1 Treatment?, *Obes. Rev.*, 2011, **12**(8), 593–601, DOI: 10.1111/j.1467-789X.2011.00860.x.

4 M. A. Sánchez-Garrido, S. J. Brandt, C. Clemmensen, T. D. Müller, R. D. DiMarchi and M. H. Tschöp, GLP-1/Glucagon Receptor Co-Agonism for Treatment of Obesity, *Diabetologia*, 2017, **60**(10), 1851–1861, DOI: 10.1007/s00125-017-4354-8.

5 K. H. Sheahan, E. A. Wahlberg and M. P. Gilbert, An Overview of GLP-1 Agonists and Recent Cardiovascular Outcomes Trials, *Postgrad. Med. J.*, 2020, **96**(1133), 156–161, DOI: 10.1136/postgradmedj-2019-137186.

6 L. Maretty, D. Gill, L. Simonsen, K. Soh, L. Zagkos, M. Galanakis, J. Sibbesen, M. T. Iglesias, A. Secher, D. Valkenborg, J. Q. Purnell, L. B. Knudsen, A. A. Tahrani and M. Geybels, Proteomic Changes upon Treatment with Semaglutide in Individuals with Obesity, *Nat. Med.*, 2025, **31**, 267–277, DOI: 10.1038/s41591-024-03355-2.

7 T. Vilsbøll, H. Agersø, T. Krarup and J. J. Holst, Similar Elimination Rates of Glucagon-Like Peptide-1 in Obese Type 2 Diabetic Patients and Healthy Subjects, *J. Clin. Endocrinol. Metab.*, 2003, **88**(1), 220–224, DOI: 10.1210/jc.2002-021053.

8 E. M. Bech, S. L. Pedersen and K. J. Jensen, Chemical Strategies for Half-Life Extension of Biopharmaceuticals: Lipidation and Its Alternatives, *ACS Med. Chem. Lett.*, 2018, **9**(7), 577–580, DOI: 10.1021/acsmedchemlett.8b00226.

9 M. Erak, K. Bellmann-Sickert, S. Els-Heindl and A. G. Beck-Sickinger, Peptide Chemistry Toolbox – Transforming Natural Peptides into Peptide Therapeutics, *Bioorg. Med. Chem.*, 2018, **26**(10), 2759–2765, DOI: 10.1016/j.bmc.2018.01.012.

10 C. Poulsen, M. Ø. Pedersen, P. O. Wahlund, A. Sjölander, J. K. Thomsen, K. W. Conde-Frieboes, J. F. Paulsson, B. S. Wulff and S. Østergaard, Rational Development of Stable PYY3-36 Peptide Y2 Receptor Agonists, *Pharm. Res.*, 2021, **38**(8), 1369–1385, DOI: 10.1007/s11095-021-03077-x.

11 S. L. Anderson, T. R. Beutel and J. M. Trujillo, Oral Semaglutide in Type 2 Diabetes, *J. Diabetes Complications*, 2020, **34**(4), 107520, DOI: 10.1016/j.jdiacomp.2019.107520.

12 E. Přáda Brichtová, I. A. Edu, X. Li, F. Becher, A. L. Gomes Dos Santos and S. E. Jackson, Effect of Lipidation on the Structure, Oligomerization, and Aggregation of Glucagon-like Peptide 1, *Bioconjugate Chem.*, 2025, acs.bioconjchem.4c00484, DOI: 10.1021/acs.bioconjchem.4c00484.

13 S.-T. Kuo, Z. Xi, X. Cong, X. Yan and D. H. Russell, Dissecting Hidden Liraglutide Oligomerization Pathways via Direct Mass Technology, Electron-Capture Dissociation, and Molecular Dynamics, *Anal. Chem.*, 2025, **97**(25), 13465–13473, DOI: 10.1021/acs.analchem.5c01851.

14 J. R. Bothe, A. Andrews, K. J. Smith, L. A. Joyce, Y. Krishnamachari and S. Kashi, Peptide Oligomerization Memory Effects and Their Impact on the Physical Stability of the GLP-1 Agonist Liraglutide, *Mol. Pharmaceutics*, 2019, **16**(5), 2153–2161, DOI: 10.1021/acs.molpharmaceut.9b00106.

15 Y. Wang, A. Lomakin, S. Kanai, R. Alex and G. B. Benedek, Transformation of Oligomers of Lipidated Peptide Induced by Change in pH, *Mol. Pharmaceutics*, 2015, **12**(2), 411–419, DOI: 10.1021/mp500519s.

16 B. Yang, D. Devalla, S. Sonzini, M. Boberg, S. Gopaul, M. Sundqvist, I. Grant, C. Jones, S. Brookes, C. Weidauer, E. Paladino, N. Mahmoudi, J. Van Rooyen, A. G. Dos Santos, J. Laru, A. Campbell, L. Jermutus and A. Bak, Cotadutide Reversible Self-Assembly Based Long-Acting Injectable Depot for Sustained Delivery of GLP-1 Glucagon Receptor Agonists with Controlled Burst Release, *J. Controlled Release*, 2025, **380**, 647–663, DOI: 10.1016/j.jconrel.2025.01.064.

17 Q. Li, V. Tangry, D. P. Allen, K. D. Seibert, K. K. Qian and N. J. Wagner, Surface-Mediated Spontaneous Emulsification of the Acylated Peptide Semaglutide, *Proc. Natl. Acad. Sci. U. S. A.*, 2024, **121**(5), e2305770121, DOI: 10.1073/pnas.2305770121.

18 I. W. Hamley, L. R. De Mello, V. Castelletto, T. Zinn, N. Cowieson, J. Seitsonen and T. Bizien, Semaglutide Aggregates into Oligomeric Micelles and Short Fibrils in Aqueous Solution, *Biomacromolecules*, 2025, **26**(6), 3786–3794, DOI: 10.1021/acs.biomac.5c00342.

19 A. Ghosh, C. J. Buettner, A. A. Manos, A. J. Wallace, M. F. Tweedle and J. E. Goldberger, Probing Peptide Amphiphile Self-Assembly in Blood Serum, *Biomacromolecules*, 2014, **15**(12), 4488–4494, DOI: 10.1021/bm501311g.

20 L. L. Lock, C. D. Reyes, P. Zhang and H. Cui, Tuning Cellular Uptake of Molecular Probes by Rational Design of Their Assembly into Supramolecular Nanoprobes, *J. Am. Chem. Soc.*, 2016, **138**(10), 3533–3540, DOI: 10.1021/jacs.6b00073.

21 Y. Kim, W. Li, S. Shin and M. Lee, Development of Toroidal Nanostructures by Self-Assembly: Rational Designs and Applications, *Acc. Chem. Res.*, 2013, **46**(12), 2888–2897, DOI: 10.1021/ar400027c.

22 H. A. Lashuel, D. Hartley, B. M. Petre, T. Walz and P. T. Lansbury, Amyloid Pores from Pathogenic Mutations, *Nature*, 2002, **418**(6895), 291, DOI: 10.1038/418291a.

23 W. Li, J. Li and M. Lee, Fabrication of Artificial Toroid Nanostructures by Modified β-Sheet Peptides, *Chem. Commun.*, 2013, **49**(74), 8238, DOI: 10.1039/c3cc44238a.

24 Y. Lim, E. Lee and M. Lee, Toroidal Nanostructures from Self-Assembly of Block Copolypeptides Based on Poly(L-Arginine) and β-Sheet Peptide, *Macromol. Rapid Commun.*, 2011, **32**(2), 191–196, DOI: 10.1002/marc.201000512.

25 Y. Lim, K. Moon and M. Lee, Stabilization of an α Helix by β-Sheet-Mediated Self-Assembly of a Macrocyclic Peptide, *Angew. Chem., Int. Ed.*, 2009, **48**(9), 1601–1605, DOI: 10.1002/anie.200804665.

 This journal is © The Royal Society of Chemistry 2025

Open Access Article. Published on 11 November 2025. Downloaded on 1/31/2026 6:07:50 AM.
This article is licensed under a Creative Commons Attribution-NonCommercial 3.0 Unported Licence.

26 K. L. Zapadka, F. J. Becher, S. Uddin, P. G. Varley, S. Bishop, A. L. Gomes dos Santos and S. E. Jackson, A pH-Induced Switch in Human Glucagon-like Peptide-1 Aggregation Kinetics, *J. Am. Chem. Soc.*, 2016, **138**(50), 16259–16265, DOI: 10.1021/jacs.6b05025.

27 I. W. Hamley, A. Adak and V. Castelletto, Influence of Chirality and Sequence in Lysine-Rich Lipopeptide Biosurfactants and Micellar Model Colloid Systems, *Nat. Commun.*, 2024, **15**(1), 6785, DOI: 10.1038/s41467-024-51234-8.

28 J. A. Hutchinson, S. Burholt, I. W. Hamley, A. K. Lundback, S. Uddin, A. Gomes Dos Santos, M. Reza, J. Seitsonen and J. Ruokolainen, The Effect of Lipidation on the Self-Assembly of the Gut-Derived Peptide Hormone PYY 3-36, *Bioconjugate Chem.*, 2018, **29**(7), 2296–2308, DOI: 10.1021/acs.bioconjchem.8b00286.

29 V. Castelletto, I. W. Hamley, J. Seitsonen, J. Ruokolainen, G. Harris, K. Bellmann-Sickert and A. G. Beck-Sickinger, Conformation and Aggregation of Selectively PEGylated and Lipidated Gastric Peptide Hormone Human PYY 3-36, *Biomacromolecules*, 2018, **19**(11), 4320–4332, DOI: 10.1021/acs.biomac.8b01209.

30 I. W. Hamley, V. Castelletto, C. Rowding, C. Wilkinson, L. R. De Mello, B. Mendes, G. Barrett and J. Seitsonen, Diverse Nanostructures and Antimicrobial Activity of Lipopeptides Bearing Lysine-Rich Tripeptide Sequences, *Soft Matter*, 2025, **21**, 6058, DOI: 10.1039/d5sm00432b.

31 C. Poulsen, M. Norrman, J. K. Thomsen and P.-O. Wahlund, Structure, Self-Association, and Aggregation Properties of a Long-Acting Amylin Receptor Agonist, *Mol. Pharmaceutics*, 2025, **22**(7), 3900–3909, DOI: 10.1021/acs.molpharmaceut.5c00161.

32 A. Miller, J. Wei, S. Meehan, C. M. Dobson, M. E. Welland, D. Klenerman, M. Vendruscolo, F. S. Ruggeri and T. P. J. Knowles, Formation of Amyloid Loops in Brain Tissues Is Controlled by the Flexibility of Protofibril Chains, *Proc. Natl. Acad. Sci. U. S. A.*, 2023, **120**(21), e2216234120, DOI: 10.1073/pnas.2216234120.

33 D. M. Hatters, C. A. MacRaild, R. Daniels, W. S. Gosal, N. H. Thomson, J. A. Jones, J. J. Davis, C. E. MacPhee, C. M. Dobson and G. J. Howlett, The Circularization of Amyloid Fibrils Formed by Apolipoprotein C-II, *Biophys. J.*, 2003, **85**(6), 3979–3990, DOI: 10.1016/S0006-3495(03)74812-7.

34 D. M. Hatters, C. E. MacPhee, L. J. Lawrence, W. H. Sawyer and G. J. Howlett, Human Apolipoprotein C-II Forms Twisted Amyloid Ribbons and Closed Loops, *Biochemistry*, 2000, **39**(28), 8276–8283, DOI: 10.1021/bi000002w.

35 B. Manandhar and J.-M. Ahn, Glucagon-like Peptide-1 (GLP-1) Analogs: Recent Advances, New Possibilities, and Therapeutic Implications, *J. Med. Chem.*, 2015, **58**(3), 1020–1037, DOI: 10.1021/jm500810s.

36 A. D. Keith, E. P. Brichtová, J. G. Barber, D. J. Wales, S. E. Jackson and K. Röder, Energy Landscapes and Structural Ensembles of Glucagon-like Peptide-1 Monomers, *J. Phys. Chem. B*, 2024, **128**(23), 5601–5611, DOI: 10.1021/acs.jpcb.4c01794.

37 X. Zhang, M. J. Belousoff, P. Zhao, A. J. Kooistra, T. T. Truong, S. Y. Ang, C. R. Underwood, T. Egebjerg, P. Šenel, G. D. Stewart, Y.-L. Liang, A. Glukhova, H. Venugopal, A. Christopoulos, S. G. B. Furness, L. J. Miller, S. Reedtz-Runge, C. J. Langmead, D. E. Gloriam, R. Danev, P. M. Sexton and D. Wootten, Differential GLP-1R Binding and Activation by Peptide and Non-Peptide Agonists, *Mol. Cell*, 2020, **80**(3), 485–500, DOI: 10.1016/j.molcel.2020.09.020.

38 S. Kirkham, V. Castelletto, I. W. Hamley, K. Inoue, R. Rambo, M. Reza and J. Ruokolainen, Self-Assembly of the Cyclic Lipopeptide Daptomycin: Spherical Micelle Formation Does Not Depend on the Presence of Calcium Chloride, *ChemPhysChem*, 2016, 2118–2122, DOI: 10.1002/cphc.201600308.

39 J. S. Lin, L. A. Bekale, N. Molchanova, J. E. Nielsen, M. Wright, B. Bacacao, G. Diamond, H. Jenssen, P. L. Santa Maria and A. E. Barron, Anti-Persister and Anti-Biofilm Activity of Self-Assembled Antimicrobial Peptoid Ellipsoidal Micelles, *ACS Infect. Dis.*, 2022, **8**, 1823–1830, DOI: 10.1021/acsinfecdis.2c00288.

40 I. W. Hamley, Self-Assembly of Amphiphilic Peptides, *Soft Matter*, 2011, **7**(9), 4122, DOI: 10.1039/c0sm01218a.

41 M. Makowska, A. Wardowska, M. Bauer, D. Wyrzykowski, I. Małuch and E. Sikorska, Impact of Lipidation Site on the Activity of α-Helical Antimicrobial Peptides, *Bioorg. Chem.*, 2024, **153**, 107821, DOI: 10.1016/j.bioorg.2024.107821.

42 Y.-H. Chen, J. T. Yang and K. H. Chau, Determination of the Helix and β Form of Proteins in Aqueous Solution by Circular Dichroism, *Biochemistry*, 1974, **13**(16), 3350–3359.

43 V. Muñoz and L. Serrano, Elucidating the Folding Problem of Helical Peptides Using Empirical Parameters. III. Temperature and pH Dependence, *J. Mol. Biol.*, 1995, **245**(3), 297–308, DOI: 10.1006/jmbi.1994.0024.

44 V. Boreikaite, B. I. M. Wicky, I. N. Watt, J. Clarke and J. E. Walker, Extrinsic Conditions Influence the Self-Association and Structure of IF1, the Regulatory Protein of Mitochondrial ATP Synthase, *Proc. Natl. Acad. Sci. U. S. A.*, 2019, **116**(21), 10354–10359, DOI: 10.1073/pnas.1903535116.